Online Supplement Information and Data

Adenylyl cyclase 5-generated cAMP controls cerebral vascular reactivity during diabetic hyperglycemia

Arsalan U. Syed[1*], Gopireddy R. Reddy[1*], Debapriya Ghosh[1*], Maria Paz Prada[1], Matthew A. Nystoriak[2], Stefano Morotti[1], Eleonora Grandi[1], Padmini Sirish[3], Nipavan Chiamvimonvat[1, 3, 5], Johannes W. Hell[1], Luis F. Santana[4], Yang K. Xiang[1,5], Madeline Nieves-Cintrón[1#] and Manuel F. Navedo[1#]

[1]Department of Pharmacology, University of California Davis, Davis, CA 95616, [2]Diabetes and Obesity Center, Department of Medicine, University of Louisville, Louisville, KY 40202, [3]Department of Internal Medicine, University of California Davis, Davis, CA 95616, [4]Department of Physiology & Membrane Biology, University of California Davis, Davis, CA 95616, and [5]VA Northern California Healthcare System, Mather, CA 95655

Supplemental Materials and Methods

Animals: Age-matched (5-8 weeks), male C57BL/6J wild type, $AC5^{-/-}$ and $AC6^{-/-}$ mice were used. Both $AC5^{-/-}$ and $AC6^{-/-}$ have been backcrossed for 10 generations into the C57BL/6J background (1). We also generated/used $AC5^{-/+}$ by crossing C57BL/6J wild type with $AC5^{-/-}$ mice. A subgroup of mice was put on either a low-fat diet (LFD; 10% kcal; D12450J) or high-fat diet (HFD; 60% kcal; D12492) (Research Diets, New Brunswick, NJ) starting at 5 weeks of age. Mice were maintained on these diets for 12 to 16 weeks. We are using this established model of type 2 diabetes because it does not depend on genetic manipulations or chemical destruction of pancreatic β cells, and it closely recapitulates clinical features of the human diabetic condition, including obesity, hyperglycemia, and hypertension (2-10). For other experiments, age-matched (8-12 weeks), wild type and $AC5^{-/-}$ mice were injected with low-doses of streptozotocin (STZ) to destroy pancreatic β cells and induce hyperglycemia as previously described (11). Briefly, mice were fasted for 6 hours followed by a single intraperitoneal (IP) injection of 50 mg/kg of STZ dissolved in 50 mM sodium citrate buffer. Control mice were IP injected with 50 mM sodium citrate buffer only (sham). This injection protocol was repeated for 5 consecutive days. During this period, the drinking water was supplemented with 10 % sucrose by volume. Mice were kept under observation for 10 days post injection regime. Blood glucose and weight were measured on the eleventh day. STZ-treated mice with blood glucose levels over 300 mg/dL were considered hyperglycemic and therefore used for experiments. All mice were euthanized by intraperitoneal (IP) injection of pentobarbital (250mg/kg). For metabolic characterization, blood samples from LFD, HFD, sham and STZ mice were analyzed at the UC Davis Mouse Biology Program facility. Cerebral arteries were dissected and placed in ice-cold nominally Ca^{2+} ringer solution (mM) 5 KCl, 140 NaCl, 2 $MgCl_2$, 10 HEPES, and 10 D-glucose adjusted to pH 7.4 with 1 M NaOH) as previously described (2-4). For some molecular biology experiments (i.e. immunoblots), whole brains were used.

Arterial myocyte isolation. Mouse cerebral arteries were dissected in ice-cold dissection buffer containing (in mM): 140 NaCl, 5 KCl, 2 $MgCl_2$, 10 D-glucose, 10 HEPES, pH 7.4, with NaOH. Arteries were digested in dissection buffer containing papain (1 mg/mL) and dithiothreitol (1 mg/mL) at 37° C for 7 min, followed by incubation in dissection buffer containing collagenase type F (0.7 mg/mL) and collagenase type H (0.3 mg/mL) at 37° C for 7 min. Arteries were washed in ice-cold dissection buffer and gently triturated with glass pipettes to disperse the cells, which were kept in ice-cold dissection buffer and used the same day.

For unpassaged, cultured mouse arterial myocytes, mouse aortas were dissected out and placed in ice-cold DMEM containing 1X glutamate, 1X pyruvate, 1X penicillin/streptavidin and fungizone (0.25 g/ml). Aorta segments were subsequently transferred and incubated in a DMEM solution containing 2.2 mg/mL of collagenase Type 2 (Worthington) at 37° C for 15 minutes to remove the adventitia. To disperse and unpassaged, cultured arterial myocytes, the tissue was cut into 2-5 mm segments and incubated at 37° C in a buffer containing (in mM): 134 NaCl, 6 KCl, $CaCl_2$, 10 HEPES, and 7 D-glucose supplemented with 2.2 mg/mL of collagenase Type 2 (Worthington) with constant shaking. The digestion was stopped by adding an equal volume of DMEM containing 5% fetal bovine serum. The digested tissue was then centrifuged for 5 minutes at 14,000 rpm. The pellet containing the digested tissue was resuspended in DMEM containing 1X glutamate, 1X pyruvate, 5% serum and 5 mM D-glucose with gentle resuspension, which resulted in dispersion of individual arterial myocytes. Cells were then seeded on glass coverslips coated with laminin and kept in an incubator at 37° C with 5% CO_2 for 2-3 days before adenoviral transduction.

Flow cytometry

Single cells were filtered through 200 μm cell strainer, fixed in 0.4% paraformaldehyde and treated with AlexaFluor 488-conjugated anti-α smooth muscle actin (Abcam, Cambridge, MA), phytoerythrin-conjugated anti-Thy1.2 (BD Bioscience, San Diego, CA), anti-CD31 (BD Bioscience), anti-CD45 (BD Bioscience, San Diego, CA) antibodies and lineage antibody cocktail (CD3e, CD11b, Cd45R, Ly-6C, Ly-6G and TER-119, BD Bioscience, San Diego, CA) in PBS with 5% donkey serum and 20 μg/mL DNAse-free RNAse (Sigma) overnight at 4° C. Cells were also stained with 40 μg/mL 7-aminoactinomycin D (7AAD, BD Bioscience, San Jose, CA) to measure the DNA content. Data were collected using a standard FACScan cytometer (BD Biosciences, San Jose, CA) upgraded to a dual laser system with the addition of a blue laser (15mW at 488nm) and a red laser (25mW at 637nm Cytek Development, Inc, Fremont, CA). Data were acquired and analyzed using CellQuest (BD Bioscience, San Diego, CA) and FlowJo software (ver9.7 Treestar Inc., San Carlos, CA), respectively.

Adenovirus infection of arterial myocytes and FRET. Laminin (Life Technologies, Grand Island, NY) diluted 100x in sterile-filtered PBS (in mM: 137 NaCl, 2.7 KCl, 10 Na_2HPO_4, 1.8 KH_2PO_4, pH = 7.4) was used to coat #0 glass coverslips (Karl Hecht, Sondheim, Germany). After adding diluted laminin (100 μL per coverslip), coverslips were placed in a 37° C incubator

with 5% CO_2 for a minimum of 2 h, then moved to a 24-well plate (Falcon, Tewksbury, MA), and washed 3x with sterile-filtered PBS. Mouse aortic cells were plated on the laminin-coated coverslips with 500 µL of serum-containing media for 48 h in a 37° C incubator with 5% CO_2. Media was then replaced with 500 µL of serum-free media-containing virus coding for the membrane-targeted Epac1-camps-based FRET sensor (ICUE3-PM) (12, 13) and placed at 37° C with 5% CO_2 for another 36 h. Viruses were produced using the AdEasy system (Qbiogene, Carlsbad, CA) (14). After infection, media was changed to serum-free media without virus. Glass coverslips were transferred to glass bottom culture dishes (MatTek, Ashland, MA) containing 3 mL PBS at room temperature.

A Zeiss AXIO Observer A1 inverted fluorescence microscope (San Diego, CA) equipped with a Hamamatsu Orca-Flash 4.0 digital camera (Bridgewater, NJ) and controlled by Metaflor software (Molecular Devices, Sunnyvale, CA) acquired phase contrast, CFP480, and FRET images. Phase contrast and CFP480 images were collected with 20x and 40x oil immersion objective lenses, while FRET images were collected using only the 40x oil immersion objective lens. Images for FRET analysis were recorded by exciting the donor fluorophore at 430-455 nm and measuring emission fluorescence with two filters (475DF40 for cyan and 535DF25 for yellow). Images were subjected to background subtraction and acquired every 30 s with exposure time of 200 ms for each channel. The donor/acceptor FRET ratio was calculated and normalized to the ratio value of baseline with 10 mM D-glucose. CFP480 images were acquired by exciting the donor fluorophore at 430-455 nm and measuring emission fluorescence with the 475DF40 filter for 25 ms. Averages of normalized curves and maximal response to stimulation were graphed based on FRET ratio changes. The decrease in ratio of YFP/CFP represented the binding of cAMP to the ICUE3-PM and was interpreted as an increase in cAMP levels. Experiments were performed at room temperature (22-25° C).

Transfection of arterial myocytes and confocal imaging: Coverslips (25 mm) were coated with cell-tak (both items from Fisher Scientific, Hampton, NH) for a minimum of 3 hours. Unpassaged, primary cultured arterial myocytes were seeded on cell-tak coated coverslips and allowed to settle for ~3 hours in an incubator at 37° C with 5% CO_2. The coverslips were then placed in 35 mm culture dishes with 3 mL of DMEM medium. After reaching 70% confluency, cells were transfected with DNA constructs (1 µg DNA) for either the general endoplasmic reticulum marker Sec61β-GFP (GenBank ID: NM_006808; kind gift from Dr. Eammon J. Dickson, Department of Physiology & Membrane Biology, University of California Davis, Davis,

CA) as well as the Epac1-camps-based FRET sensor (ICUE3) targeted to the plasma membrane (ICUE3-PM) or the nucleus (ICUE3-NLS) (12, 13) using TransfeX transfection reagents following the manufacturer's instructions (ATCC, Manassas, VA). An Olympus FV1000 confocal microscope paired with an Olympus 60x oil immersion lens (NA = 1.4) was used to collect images at different optical planes (z-axis – 0.5 µm) of the GFP and YFP fluorescence associated with the Sec61β as well as ICUE3-PM and ICUE3-NLS constructs, respectively. Images were processed offline using the NIH ImageJ open software (4, 15).

Arterial diameter measurements: Freshly isolated cerebral artery segments, approximately 1 mm in length, were cannulated on the glass micropipettes in a 5 mL myograph chamber as described previously (2-4). The arteries were equilibrated at 20 mmHg and continuously superfused (37° C, 30 min, 3 to 5 mL/min) with artificial cerebral spinal fluid (aCSF) solution containing (in mM): 119 NaCl, 4.7 KCl, 2 $CaCl_2$, 24 $NaHCO_3$, 1.2 KH_2PO_4, 1.2 $MgSO_4$, and 10 D-glucose. The aCSF solution was aerated with 5% CO_2/95% O_2 to maintain the pH between 7.35-7.40. After equilibration, arteries were exposed to 60 mM K^+ aCSF (isosmotic replacement of NaCl with KCl) to test for viability. Only arteries that constricted >50% were used for this study. Viable arteries were pressurized to 60 mmHg and equilibrated at this intravascular pressure for 1 h. Arteries that developed stable myogenic tone were used for this study. Once the arteries had achieved stable diameter, vessels were submitted to the different treatment conditions. In a set of experiments, arteries were submitted to a range of intravascular pressures from 10 mmHg to 100 mmHg. Passive diameter was obtained in Ca^{2+} free aCSF solution with 1 µM nifedipine (0 Ca^{2+}/nif). The myogenic tone percentage was calculated using the following equation: [(DP-DA)/DP]*100, where DP = passive (in 0 Ca^{2+}/nif aCSF solution) diameter and DA = active (in Ca^{2+} containing aCSF solution) diameter.

Electrophysiology: All experiments were performed at room temperature (22-25° C). Whole-cell data were acquired using an Axopatch 200B amplifier and Digidata 1440 digitizer (Molecular Devices). Recording electrodes were pulled from borosilicate capillary glass using a micropipette puller (model P-97, Sutter Instruments) and subsequently polished to achieve resistances that ranged from 3-4 MΩ. Whole-cell currents were assessed in freshly dissociated arterial myocytes using the perforated whole-cell mode of the patch-clamp technique with Ba^{2+} as a charge carrier (I_{Ba}) after myocytes were allowed to attach (10 min) to a glass coverslip in a recording chamber. Borosilicate glass pipettes were filled with a solution containing (in mM): 120 CsCl, 20 tetraethylammonium chloride (TEA-Cl), 1 EGTA, and 20 HEPES with amphotericin

B (250 µg/mL; pH adjusted to 7.2 with CsOH). The bath solution consisted of (in mM): 115 NaCl, 10 TEA-Cl, 0.5 $MgCl_2$, 10 D-glucose, 5 CsCl, 20 $BaCl_2$, and 20 HEPES (pH adjusted to 7.4 with CsOH). The I-V relationship of nifedipine-sensitive I_{Ba} was determined by 200 ms depolarizing steps from -70 mV to voltages ranging from -60 to +60 mV in increments of +10 mV. Currents were sampled at 10 kHz and low pass-filtered at 5 kHz. The L-type $Ca_V1.2$ blocker nifedipine (1 µM) was applied at the end of each experiment to determine the nifedipine-sensitive component. The I-V relationship for averaged datasets was fit with a peak Gaussian function: $I(V) = I_{max} \times \exp(-0.5((V - V_{max})/b)^2)$, where I_{max} is peak I, V_{max} is V at I_{max}, and b is the slope of the distribution, as previously described (4). In a set of experiments, I_{Ba} were elicited by voltage ramps from -80 mV to +40 mV. A voltage error of 10 mV attributable to the liquid junction potential of the recording solutions was corrected offline. All experiments were first performed in the presence of 10 mM D-glucose under static bath conditions. For the acute exposure experiments, this solution was then exchanged for a solution containing 20 mM D-glucose at a rate of 2.1 mL/min. Flow was stopped after 3 minutes, and I_{Ba} were recorded again under static flow conditions at least 5 minutes after the indicated treatment was initiated. For some experiments, arterial myocytes were pretreated for 10-15 minutes with indicated inhibitors prior to I_{Ba} recordings.

Proximity ligation assay: Duolink In Situ proximity ligation assay (PLA) kit (Sigma; (16)) was used to detect complexes containing AC5 and $Ca_V1.2$ protein in freshly isolated cerebral arterial myocytes as previously described (4, 15). Briefly, freshly isolated cells were plated on glass coverslip and left to adhere for 1 h. The cells were fixed with 4% paraformaldehyde (20 min) and quenched with 100 mM glycine (15 min). Washes (2x 3 min) were performed with PBS and the cells were permeabilized with 0.1% TritonX-100 (20 min). The permeabilized cells were then blocked for 1 h at 37° C with 50% Odyssey blocking solution (LI-COR Biotechnology). Primary antibodies (in antibody diluent solution containing 0.1% Odyssey blocking buffer (LI-COR Biotechnology) and 0.05% Triton X-100 in PBS) were added and kept overnight at 4° C (1:1000 goat anti-AC5 sc74301 from Santa Cruz Biotechnology, 1:100 custom rabbit anti-FP1 (17) and 1:1000 monoclonal TfR from ThermoFisher Scientific). For control, cells were incubated with a single primary antibody. After 12 h, cells were washed with Buffer A provided with the kit. The detection protocol (PLA-probes, ligation and amplification) was carried out per manufacturer instructions. The fluorescence signal was visualized using an Olympus FV1000 confocal microscope system with a 60x oil immersion lens (NA, 1.4). Images were acquired at different

optical planes (z-axis = 0.5 µm). Analysis was performed as previously described using the NIH ImageJ open software (4, 15, 18).

***In silico* modeling:** Simulations were performed using the Kapela *et al* mathematical model of electrophysiology and Ca^{2+} dynamics in arterial myocytes (19). This model integrates transmembrane ion fluxes involved in membrane potential (E_m) regulation with intracellular mechanisms controlling Ca^{2+} homeostasis. The wild type cell model has been adjusted to recapitulate known glucose-mediated changes in the conductance of L-type Ca^{2+} channels (2-fold increase), large-conductance Ca^{2+}-activated K^+ channels (58% reduction) and voltage-gated K^+ channels (63% reduction) in arterial myocytes (2-4, 20, 21), as previously described by us (22). The $AC5^{-/-}$ model was derived from a baseline model by altering the conductance of K^+ channels, but not L-type Ca^{2+} channels, to the same extent as in wild type cells. The system of ordinary differential equations was implemented in MATLAB (The MathWorks, Natick, MA, USA) and solved using the stiff ordinary differential equation solver ode15s. The code is freely available for download at: somapp.ucdmc.ucdavis.edu/Pharmacology/bers or elegrandi.wixsite.com/grandilab/downloads.

Immunolabelling and Ground State Depletion (GSD) microscopy: Freshly isolated arterial myocytes were plated and allowed to adhere to a coverslip for 1 h. Cells were washed with PBS (3x 15 min) and fixed using 3% paraformaldehyde + 0.1% glutaraldehyde solution in PBS (10 min), immediately followed by a 5 min incubation with 0.1% sodium borohydride in H_2O. After washing with PBS (3x 15 min), the fixed cells were permeabilized and blocked with 0.05% Triton X-100 and 20% SEA BLOCK (Thermo Scientific) in a PBS solution for 1 h at room temperature. Primary antibodies diluted in the blocking solution were added and kept overnight at 4° C (10 µg/mL goat anti-AC5 sc74301; Santa Cruz Biotechnology and 10 µg/mL custom rabbit anti-FP1) (17). The following day, cells were rinsed 3x and washed with PBS (3x 15 min). Secondary antibodies donkey Alexa Fluor 647 conjugated antibody recognizing goat immunoglobulin G (2 µg/mL; Molecular Probes) and donkey Alexa Fluor 568 conjugated antibody recognizing rabbit immunoglobulin G (2 µg/mL; Molecular Probes) diluted in blocking buffer were added for 1 h at room temperature. Following incubation with secondary antibodies, cells were carefully rinsed 3x and then washed with PBS (3x 15 min). Specificity of secondary antibodies was tested in control experiments in which primary antibodies were omitted from the preparation (no 1° antibody control) or non-immune isotype specific immunoglobulins (e.g. rabbit IgG or goat IgG) were used.

Imaging was performed using coverslips mounted on a round cavity microscope slide containing MEA-GLOX imaging buffer (NeoLab Migge Laborbedarf-Vertriebs GmbH, Germany) and sealed with Twinsil (Picodent, Germany). Imaging buffer composition contained 10 mM MEA (cysteamine), 0.56 mg/mL glucose oxidase, 34 µg/mL catalase, and buffer containing 10% w/v glucose, 10 mM NaCl, and 50 mM Tris-HCl, pH 8. Images were obtained using a super-resolution ground state depletion system (SR-GSD, Leica) dependent on stochastic single-molecule localization and equipped with high-power lasers (532 nm 2.1 kW/ cm^2; 642 nm 2.1 kW/ cm^2; 405 nm 30 mW). A 160x HCX Plan-Apochromat (NA 1.47) oil immersion lens and an electron-multiplying charge-coupled device (EMCCD) camera (iXon3 897; Andor Technology) were used to acquire images. The camera was running in frame-transfer mode at a frame rate of 100 Hz (10 ms exposure time). Fluorescence was detected through Leica high-power TIRF filter cubes (532 HP-T, 642 HP-T) with emission band-pass filters of 550-650 nm and 660-760 nm.

AC5 and $Ca_V1.2$ distributions were reconstructed from 30,000 images using the coordinates of centroids obtained by fitting single-molecule fluorescence signals with a 2D Gaussian function in LASAF software (Leica). The localization accuracy of the system is limited by the statistical noise of photon counting; the precision of localization is proportional to DLR/√N, where DLR is the diffraction-limited resolution of a fluorophore and N is the average number of detected photons per switching event, assuming the point-spread functions are Gaussian (23, 24). The full width at half maximum for single-molecule signals was ~20 nm (25). Localizations produced from less than 800 photons were filtered out of the reconstruction. All pixels with intensity above a user-defined threshold were binarized and segmented into individual objects and included as clusters in our analysis. Cluster size and density were determined using the Analyze Particle option in the ImageJ software (National Institute of Health). The JACoP plug-in in the ImageJ software was used to automatically determine the shortest intermolecular distances for $Ca_V1.2$ and AC5 following the protocol described by (26). Intermolecular distance histograms were generated from the JACoP plug-in output data and fitted with a sum of two Gaussian functions of the following equation: $Y = Y_0 + (A_1 / (w_1 \times \sqrt{(\pi/2)})) \times \exp(-2 \times ((X - X_{C1})/ w_1)^2) + (A_2 / (w_2 \times \sqrt{(\pi/2)})) \times \exp(-2 \times ((X - X_{C2})/ w_2)^2)$, where Y_0 is the Y offset, A_1 and A_2 are the areas of the distribution of distances, X_{C1} and X_{C2} are the x values of distance at the center of the distribution, and w_1 and w_2 are the widths of each distribution in nanometers.

Immunoblotting: Freshly isolated mouse whole brains were homogenized in a RIPA lysis buffer solution (mM); 50 Tris base, 150 NaCl, 5 EGTA, 10 EDTA, 1% nonyl phenoxypolyethoxylethanol-40 (NP-40), 10% glycerol, 0.05% sodium dodecyl sulfate (SDS), 0.4% deoxycholic acid (DOC) with protease inhibitors (1 µg/mL pepstatin A, 10 µg/mL leupeptin, 20 µg/mL aprotinin, and 200 nM phenylmethylsulfonyl fluoride). The lysate was then cleared by centrifugation (250,000 X g, 30 min, 4° C). The resulting supernatant was used as the whole brain lysate. Samples were boiled in Laemmli Sample Buffer (Bio-Rad) for 5 min at 95° C. Proteins were separated by SDS-polyacrylamide gel electrophoresis (75-100 V; 1.5 h) in a separating phase polymerized from 3% acrylamide and a resolving phase polymerized from 7.5% acrylamide. Separated proteins were then transferred to a polyvinylidene difluoride membrane (50 V, 600 min, 4° C). Membranes were blocked in 5% nonfat dried milk in tris-buffered saline with 0.05% Tween 20 (TBS-T) (1 h, room temperature) and then incubated in primary antibody (3 h, room temperature). Antibodies were diluted in 5% nonfat dried milk in TBS-T (1:500 goat anti-AC5 sc74301 from Santa Cruz Biotechnology and 1:1000 mouse anti-β-actin from Abcam). This was followed by incubation of membrane in horseradish peroxidase-labeled goat-anti-mouse antibodies (1:10000 from Bio-Rad) and donkey-anti-goat antibodies (1:10000 from Bio-Rad;) in 5% nonfat dried milk TBS-T. Classico (Millipore) and Femto (Thermo) chemiluminescence reagents and exposure to x-ray film were used to identify the bands. Densitometry analysis for bands was performed with ImageJ software (National Institutes of Health). β-actin was used for normalization of AC5 loading input (density expressed as percentage of β-actin).

Immunofluorescence: Freshly dissociated arterial myocytes were fixed and labeled, as previously described (15, 18, 27, 28), using a goat anti-AC5 (1:1000, sc74301 from Santa Cruz Biotechnology). The secondary antibody was an Alexa Fluor 488 conjugated donkey anti-goat (5 mg/mL; Molecular Probes). Cells were imaged using an Olympus FV1000 confocal microscope paired with an Olympus 60x oil immersion lens (NA = 1.43) and a zoom of 3.0 (pixel size = 0.1 µm).

***In vivo* intravital imaging using cranial window:** Mice were anesthetized with isoflurane (5% induction, and 2 % maintenance for the duration of the surgery). Upon obtaining stage III anesthesia, the skin above the skull was removed, thus exposing the top of the cranium. A steel plate with ~2 mm diameter hole was attached on the region of interest using dental cement and superglue. The head plate was secured to a holding frame and a circular cranial window ~2 mm

in diameter was drilled in the skull. Mice were injected with ketamine (100 mg/kg) and xylazine (10 mg/kg) to replace 2% isoflurane-induced anesthesia. Body temperature was maintained at 37° C for the duration of the experiment using an electrical heating pad. *In vivo* images were acquired using a Unitron Z850 stereomicroscope and a StCamSware software (Sentech America Incorporated). Arterial diameter was analyzed using NIH ImageJ Line Measurement tool by drawing a line across the arterial walls before and after treatments. The aCSF solution was acutely added to the cranial window with either 10 mM D-glucose, 20 mM D-glucose or 10 mM D-glucose + 10 mM mannitol. Passive diameter was obtained in Ca^{2+} free aCSF solution with 1 μM nifedipine (0 Ca^{2+}/nif). The percentage myogenic tone was calculated using the following equation: [(DP-DA)/DP]*100, where DP = passive (in 0 Ca^{2+}/nif aCSF solution) diameter and DA = active (in Ca^{2+} containing aCSF solution) diameter.

Chemicals: All chemical reagents were from Sigma-Aldrich (St. Louis, MO) unless otherwise stated. A list of key reagents/resources is included in Table S15.

Statistics: Data were analyzed using GraphPad Prism software and expressed as mean ± SEM. Number of technical and biological replicates is based on previously published observations to reached statistical differences between datasets (2-4, 15, 18, 28, 29), which is consistent with the general number of replicates and conditions commonly accepted in the field. Data were assessed for potential outliers using the GraphPad Prism Outlier Test and for normality of distribution. Statistical significance was then determined using appropriate paired or unpaired two-tailed Student's *t*-test, nonparametric tests or One-way analysis of variance (ANOVA) for multiple comparisons with appropriate post hoc test. $P < 0.05$ was considered statistically significant (denoted by * in figures).

Study Approval: All animal studies strictly adhered to the approved Institutional Animal Care and Use Committee protocols (protocols #: 20321 and 20234) at the University of California, Davis.

References

1. Timofeyev, V., Myers, R.E., Kim, H.J., Woltz, R.L., Sirish, P., Heiserman, J.P., Li, N., Singapuri, A., Tang, T., Yarov-Yarovoy, V., et al. 2013. Adenylyl cyclase subtype-specific compartmentalization: differential regulation of L-type Ca^{2+} current in ventricular myocytes. *Circ Res* 112:1567-1576.
2. Nystoriak, M.A., Nieves-Cintron, M., Nygren, P.J., Hinke, S.A., Nichols, C.B., Chen, C.Y., Puglisi, J.L., Izu, L.T., Bers, D.M., Dell'acqua, M.L., et al. 2014. AKAP150 contributes to enhanced vascular tone by facilitating large-conductance Ca^{2+}-activated K^+ channel remodeling in hyperglycemia and diabetes mellitus. *Circ Res* 114:607-615.
3. Nieves-Cintron, M., Nystoriak, M.A., Prada, M.P., Johnson, K., Fayer, W., Dell'Acqua, M.L., Scott, J.D., and Navedo, M.F. 2015. Selective downregulation of $K_V2.1$ function contributes to enhanced arterial tone during diabetes. *Journal of Biological Chemistry* 290:7918-7929.
4. Nystoriak, M.A., Nieves-Cintron, M., Patriarchi, T., Buonarati, O.R., Prada, M.P., Morotti, S., Grandi, E., Fernandes, J.D., Forbush, K., Hofmann, F., et al. 2017. Ser1928 phosphorylation by PKA stimulates the L-type Ca^{2+} channel $Ca_V1.2$ and vasoconstriction during acute hyperglycemia and diabetes. *Sci Signal* 10.
5. Winzell, M.S., and Ahren, B. 2004. The high-fat diet-fed mouse: a model for studying mechanisms and treatment of impaired glucose tolerance and type 2 diabetes. *Diabetes* 53 Suppl 3:S215-219.
6. Kim, F., Pham, M., Maloney, E., Rizzo, N.O., Morton, G.J., Wisse, B.E., Kirk, E.A., Chait, A., and Schwartz, M.W. 2008. Vascular inflammation, insulin resistance, and reduced nitric oxide production precede the onset of peripheral insulin resistance. *Arterioscler Thromb Vasc Biol* 28:1982-1988.
7. Surwit, R.S., Kuhn, C.M., Cochrane, C., McCubbin, J.A., and Feinglos, M.N. 1988. Diet-induced type II diabetes in C57BL/6J mice. *Diabetes* 37:1163-1167.
8. Calligaris, S.D., Lecanda, M., Solis, F., Ezquer, M., Gutierrez, J., Brandan, E., Leiva, A., Sobrevia, L., and Conget, P. 2013. Mice long-term high-fat diet feeding recapitulates human cardiovascular alterations: an animal model to study the early phases of diabetic cardiomyopathy. *PLoS One* 8:e60931.
9. Islam, M.S., and Loots du, T. 2009. Experimental rodent models of type 2 diabetes: a review. *Methods Find Exp Clin Pharmacol* 31:249-261.
10. Heydemann, A. 2016. An Overview of Murine High Fat Diet as a Model for Type 2 Diabetes Mellitus. *J Diabetes Res* 2016:2902351.
11. Wu, K.K., and Huan, Y. 2008. Streptozotocin-induced diabetic models in mice and rats. *Curr Protoc Pharmacol* Chapter 5:Unit 5 47.
12. Allen, M.D., DiPilato, L.M., Rahdar, M., Ren, Y.R., Chong, C., Liu, J.O., and Zhang, J. 2006. Reading dynamic kinase activity in living cells for high-throughput screening. *ACS Chem Biol* 1:371-376.
13. Liu, S., Zhang, J., and Xiang, Y.K. 2011. FRET-based direct detection of dynamic protein kinase A activity on the sarcoplasmic reticulum in cardiomyocytes. *Biochem Biophys Res Commun* 404:581-586.
14. Luo, J., Deng, Z.L., Luo, X., Tang, N., Song, W.X., Chen, J., Sharff, K.A., Luu, H.H., Haydon, R.C., Kinzler, K.W., et al. 2007. A protocol for rapid generation of recombinant adenoviruses using the AdEasy system. *Nat Protoc* 2:1236-1247.
15. Nieves-Cintron, M., Syed, A.U., Buonarati, O.R., Rigor, R.R., Nystoriak, M.A., Ghosh, D., Sasse, K.C., Ward, S.M., Santana, L.F., Hell, J.W., et al. 2017. Impaired BK_{Ca} channel function in native vascular smooth muscle from humans with type 2 diabetes. *Sci Rep* 7:14058.

16. Fredriksson, S., Gullberg, M., Jarvius, J., Olsson, C., Pietras, K., Gustafsdottir, S.M., Ostman, A., and Landegren, U. 2002. Protein detection using proximity-dependent DNA ligation assays. *Nat Biotechnol* 20:473-477.
17. Davare, M.A., Horne, M.C., and Hell, J.W. 2000. Protein phosphatase 2A is associated with class C L-type Ca^{2+} channels ($Ca_V1.2$) and antagonizes channel phosphorylation by cAMP-dependent protein kinase. *J Biol Chem* 275:39710-39717.
18. Prada, M.P., Syed, A.U., Buonarati, O.R., Reddy, G.R., Nystoriak, M.A., Ghosh, D., Simo, S., Sato, D., Sasse, K.C., Ward, S.M., et al. 2019. A Gs-coupled purinergic receptor boosts Ca^{2+} influx and vascular contractility during diabetic hyperglycemia. *Elife* 8.
19. Kapela, A., Bezerianos, A., and Tsoukias, N.M. 2008. A mathematical model of Ca^{2+} dynamics in rat mesenteric smooth muscle cell: agonist and NO stimulation. *J Theor Biol* 253:238-260.
20. Rainbow, R.D., Hardy, M.E., Standen, N.B., and Davies, N.W. 2006. Glucose reduces endothelin inhibition of voltage-gated potassium channels in rat arterial smooth muscle cells. *J Physiol* 575:833-844.
21. Straub, S.V., Girouard, H., Doetsch, P.E., Hannah, R.M., Wilkerson, M.K., and Nelson, M.T. 2009. Regulation of intracerebral arteriolar tone by K_V channels: effects of glucose and PKC. *Am J Physiol Cell Physiol* 297:C788-796.
22. Morotti, S., Nieves-Cintron, M., Nystoriak, M.A., Navedo, M.F., and Grandi, E. 2017. Predominant contribution of L-type $Ca_V1.2$ channel stimulation to impaired intracellular calcium and cerebral artery vasoconstriction in diabetic hyperglycemia. *Channels (Austin)* 11:340-346.
23. Dempsey, G.T., Vaughan, J.C., Chen, K.H., Bates, M., and Zhuang, X. 2011. Evaluation of fluorophores for optimal performance in localization-based super-resolution imaging. *Nat Methods* 8:1027-1036.
24. Folling, J., Bossi, M., Bock, H., Medda, R., Wurm, C.A., Hein, B., Jakobs, S., Eggeling, C., and Hell, S.W. 2008. Fluorescence nanoscopy by ground-state depletion and single-molecule return. *Nat Methods* 5:943-945.
25. Tajada, S., Moreno, C.M., O'Dwyer, S., Woods, S., Sato, D., Navedo, M.F., and Santana, L.F. 2017. Distance constraints on activation of TRPV4 channels by AKAP150-bound PKCα in arterial myocytes. *J Gen Physiol* 149:639-659.
26. Bolte, S., and Cordelieres, F.P. 2006. A guided tour into subcellular colocalization analysis in light microscopy. *J Microsc* 224:213-232.
27. Navedo, M.F., Amberg, G.C., Nieves, M., Molkentin, J.D., and Santana, L.F. 2006. Mechanisms underlying heterogeneous Ca^{2+} sparklet activity in arterial smooth muscle. *J Gen Physiol* 127:611-622.
28. Navedo, M.F., Nieves-Cintron, M., Amberg, G.C., Yuan, C., Votaw, V.S., Lederer, W.J., McKnight, G.S., and Santana, L.F. 2008. AKAP150 is required for stuttering persistent Ca^{2+} sparklets and angiotensin II-induced hypertension. *Circ Res* 102:e1-e11.
29. Navedo, M.F., Takeda, Y., Nieves-Cintron, M., Molkentin, J.D., and Santana, L.F. 2010. Elevated Ca^{2+} sparklet activity during acute hyperglycemia and diabetes in cerebral arterial smooth muscle cells. *Am J Physiol Cell Physiol* 298:C211-220.

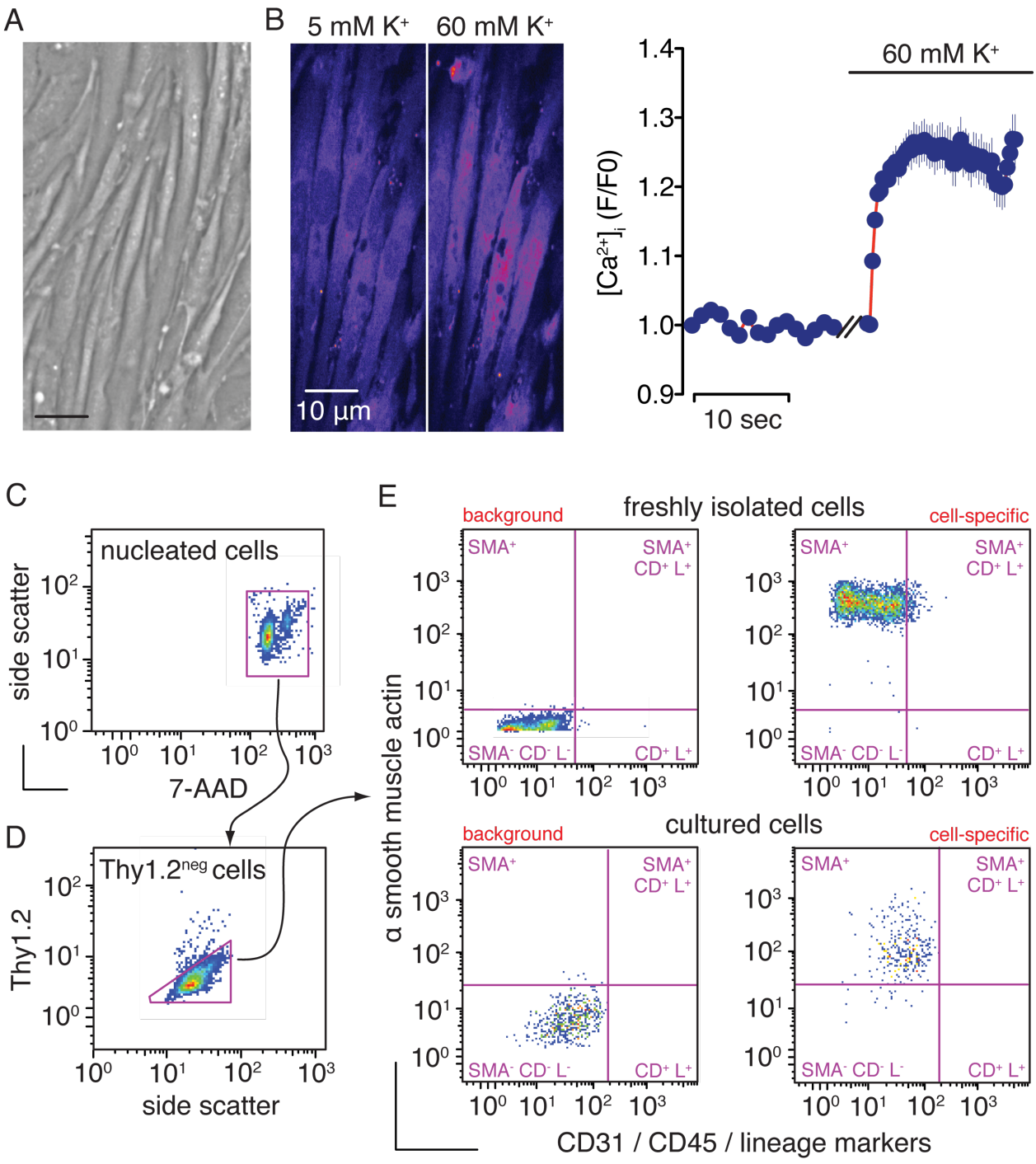

Figure S1: Primary, unpassaged arterial myocytes. A) Exemplary differential interference contrast (DIC) image of typical primary, unpassaged arterial myocytes (scale bar = 20 µm). **B)** Representative images of arterial myocytes loaded with the fluorescent Ca^{2+} indicator fluo-4 AM in the presence of 5 mM and 60 mM extracellular K^+ (*left panel*) and spatially averaged $[Ca^{2+}]_i$ (F/F_0) before and after application of 60 mM extracellular K^+ (*right panel*; n = 5 preparations). **C-**

E) Flow cytometric analyses of mouse arterial myocytes (α-SMA^{+}/Thy^{-}/CD31^{-}/CD45^{-}/Lin^{-}). Nucleated cells were selected from the mixed population based on the incorporation of 7-AAD (**C**). Panel **D** represents the selection of non-fibroblasts (Thy1.2^{neg}) cells. Arterial myocytes (**E**) were identified as CD31/CD45/lineage negative and α-smooth muscle actin positive. X and Y axes represent arbitrary units. Representative results from 2 preparations are shown. Data are represented as mean ± SEM.

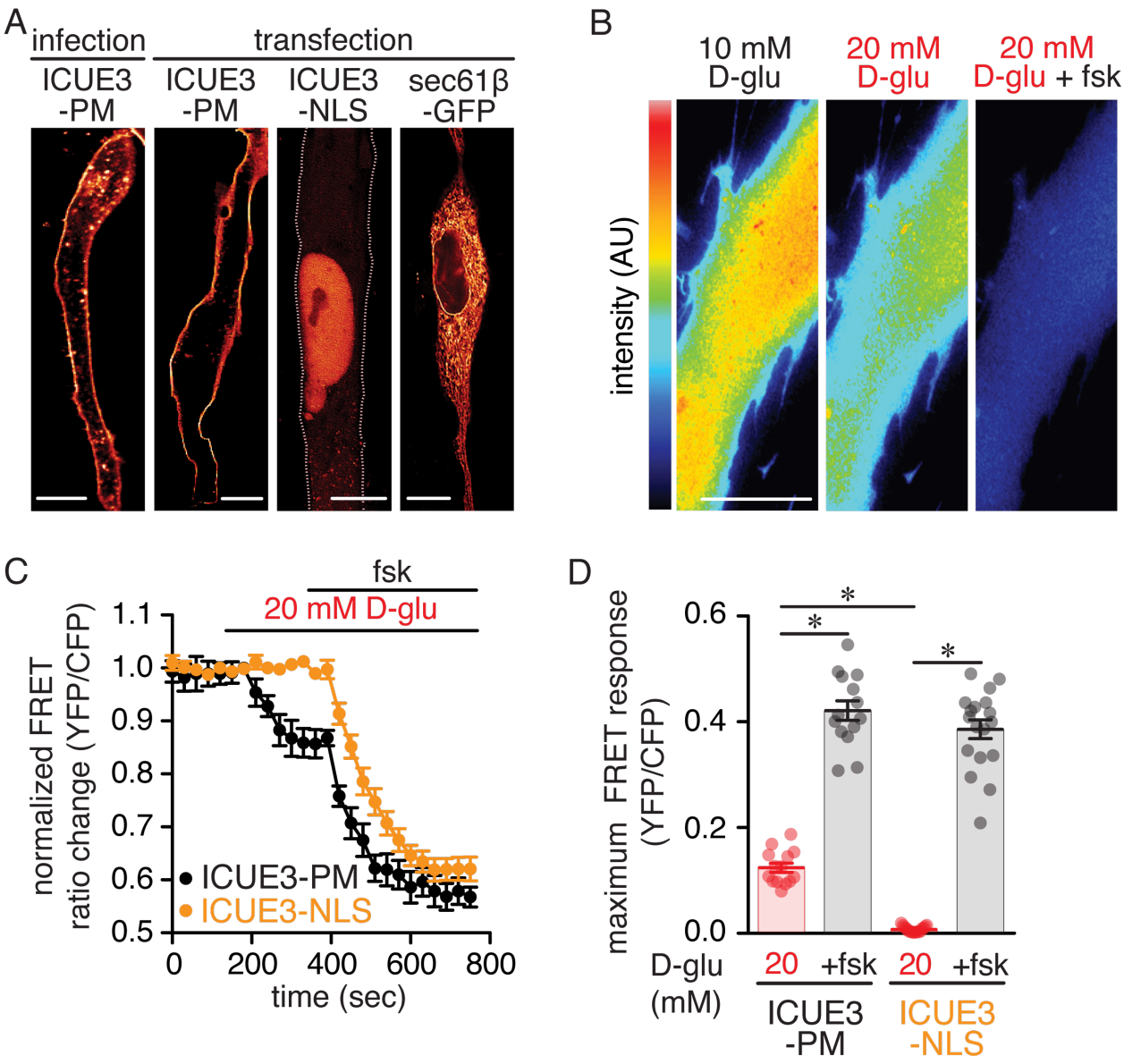

Figure S2: Targeting and readout of ICUE3 sensors in arterial myocytes. A) Representative confocal images in a single z plane of single arterial myocytes infected with the ICUE3-PM sensor or transfected with ICUE3-PM and ICUE3-NLS as well as the ER marker sec61β-GFP (scale bar = 5 µm). **B)** Representative pseudo-colored wide-field FRET ratio images of a single arterial myocyte expressing ICUE3-PM in the presence of 10 mM D-glucose, 20 mM D-glucose and 20 mM D-glucose + forskolin (1 µM) (scale bar = 3 µm). **C)** Average ICUE3-PM and ICUE3-NLS responses to increases from 10 mM to 20 mM external D-glucose before and after application of forskolin (1 µM) in wild type arterial myocytes. The FRET signals were normalized to the YFP/CFP ratio observed under control (10 mM D-glucose) conditions. **D)**

Plot of maximum FRET response (mean ± SEM) to 20 mM D-glucose and 20 mM D-glucose + 1 μM forskolin in wild type arterial myocytes expressing either ICUE3-PM (14 cells) or ICUE3-NLS (18 cells). Cells from 3 mice. *P < 0.05, Kruskal-Wallis test. Statistical differences were compared between all datasets and the asterisk highlights those with significance. Data are represented as mean ± SEM.

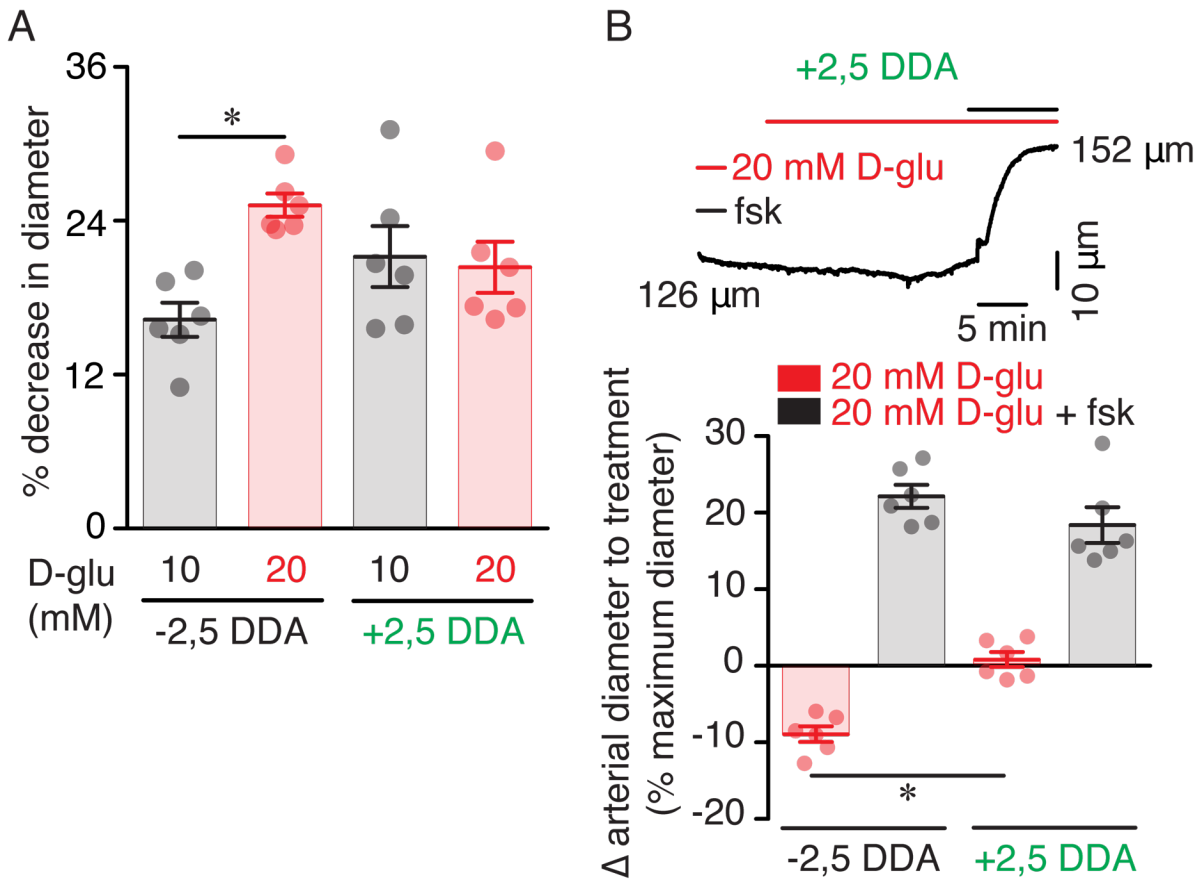

Figure S3: AC role on arterial tone in response to elevated glucose. A) Summary arterial tone data (mean ± SEM) from pressurized (60 mmHg) wild type cerebral arteries under control conditions (e.g. -2,5 DDA; n = 6 arteries from 6 mice) and arteries pre-treated with 2,5 DDA (e.g. +2,5 DDA; n = 6 arteries from 4 mice) in response to increasing extracellular glucose from 10 mM to 20 mM D-glucose. *P < 0.05, Wilcoxon matched-pairs signed-rank test. Significance was compared between 10 mM and 20 mM D-glucose for each dataset. **B)** Representative diameter recordings (*top panel*) and summary change in arterial diameter (*lower panel*; mean ± SEM) from pressurized (60 mmHg) wild type cerebral arteries untreated (n = 6 arteries from 6 mice) and pre-treated with 2,5 DDA (n = 6 arteries from 4 mice) in response to increasing extracellular glucose from 10 mM to 20 mM D-glucose or 20 mM D-glucose + 1 µM forskolin. *P < 0.05, Mann-Whitney test for comparison between the 20 mM D-glucose responses in -2,5 DDA and +2,5 DDA arteries. P = 0.1320, Mann-Whitney test for comparison between 20 mM D-glucose + forskolin responses in -2,5 DDA and +2,5 DDA arteries. Data are represented as mean ± SEM.

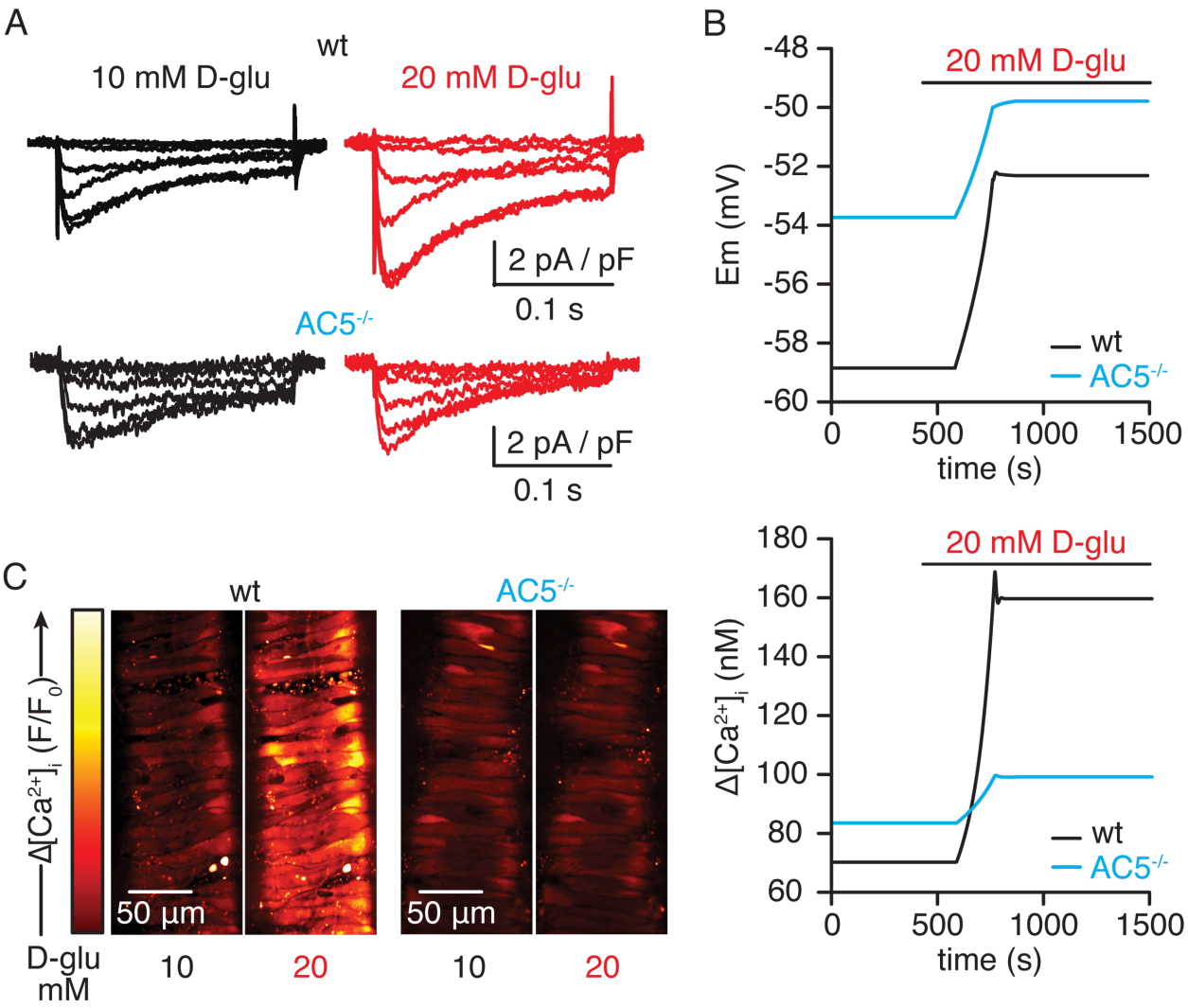

Figure S4: I_{Ba} recordings, *in silico* modeling and global $[Ca^{2+}]_i$ response to elevated glucose in wild type and AC5$^{-/-}$ cell/arteries. A) Exemplary nifedipine-sensitive I_{Ba} evoked over a range of voltages (-60 to +50 mV) in wild type (*top traces*) and AC5$^{-/-}$ (*bottom traces*) arterial myocytes before and after increasing extracellular glucose from 10 mM to 20 mM. For clarity, we are only showing traces obtained at -60, -40, -20, +10, +30 and +50 mV. **B)** Predicted variations from *in silico* modeling of wild type and AC5$^{-/-}$ arterial myocyte E_m (*top panel*) and global $[Ca^{2+}]_i$ (*lower panel*) in response to elevated glucose from 10 mM to 20 mM. **C)** Representative confocal images of wild type and AC5$^{-/-}$ arterial myocytes loaded with the Ca^{2+} indicator fluo-4 AM in intact cerebral arteries showing global $[Ca^{2+}]_i$ (F/F_0) in the presence of 10 mM or 20 mM D-glucose.

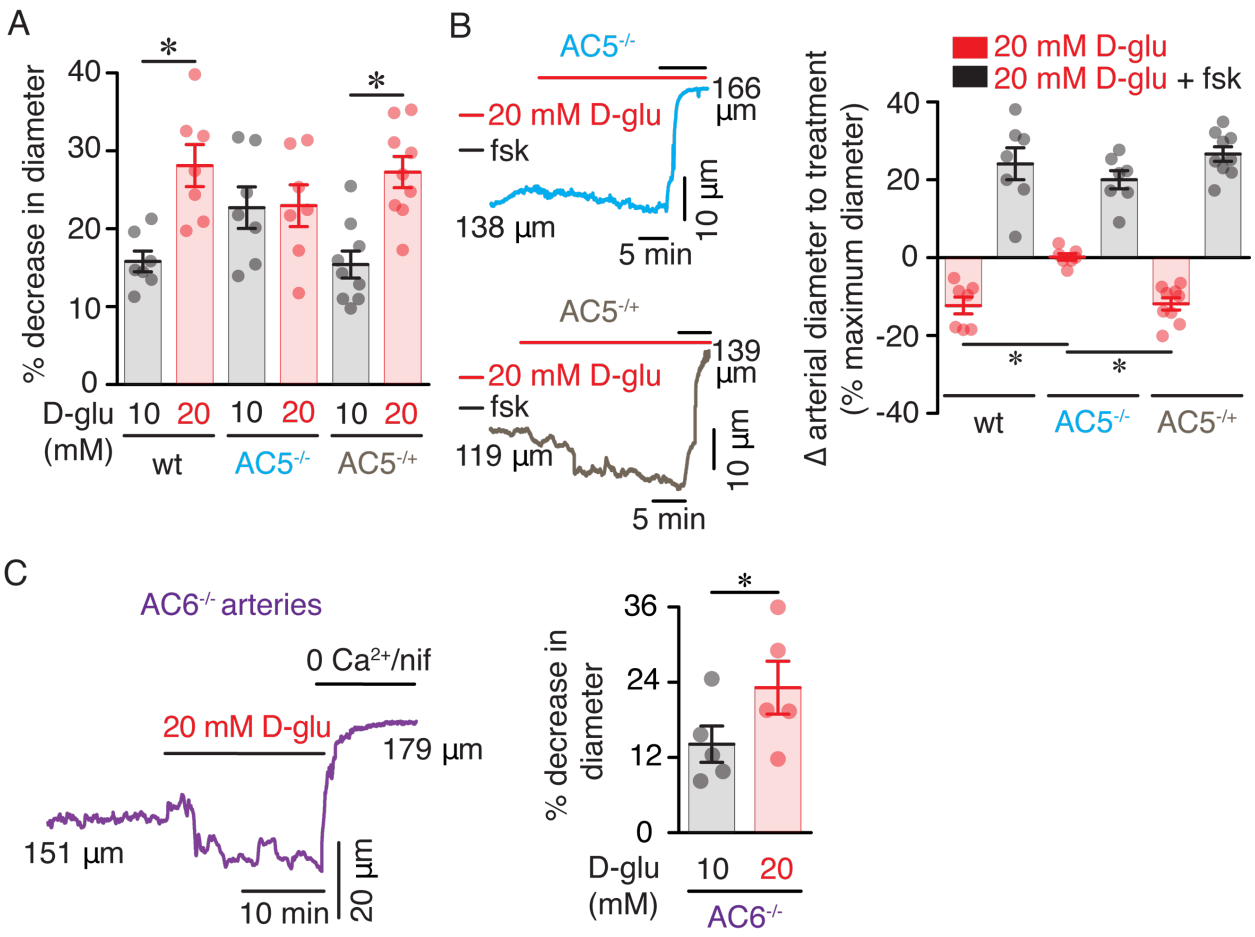

Figure S5: AC5 and AC6 role on arterial tone in response to elevated glucose. A) Summary arterial tone data (mean ± SEM) from wild type (n = 7 arteries from 4 mice), AC5$^{-/-}$ (n = 7 arteries from 7 mice) and AC5$^{-/+}$ (n = 9 arteries from 4 mice) pressurized arteries in response to increasing extracellular glucose from 10 mM to 20 mM D-glucose. *P < 0.05, Wilcoxon matched-pairs signed-rank test. Significance was compared between datasets for each group. **B)** Representative diameter recordings (*left panel*) from pressurized (60 mmHg) AC5$^{-/-}$ and AC5$^{-/+}$ cerebral arteries and summary change (mean ± SEM) in arterial diameter (*right panel*) from wild type (n = 7 arteries from 6 mice), AC5$^{-/-}$ (n = 7 arteries from 7 mice) and AC5$^{-/+}$ (n = 9 arteries from 4 mice) cerebral arteries in response to increasing extracellular glucose from 10 mM to 20 mM D-glucose or 20 mM D-glucose + 1 µM forskolin. *P < 0.05, Kruskal-Wallis test with direct comparison between the 20 mM D-glucose datasets or 20 mM D-glucose + forskolin datasets in wild type, AC5$^{-/-}$ and AC5$^{-/+}$ arteries. **C)** Representative diameter recording and plot of the myogenic tone (mean ± SEM) of AC6$^{-/-}$ arteries in the presence of 10

mM D-glucose and after application of 20 mM D-glucose (n = 5 arteries from 2 mice). *$P < 0.05$, Paired *t*-test. Data are represented as mean ± SEM.

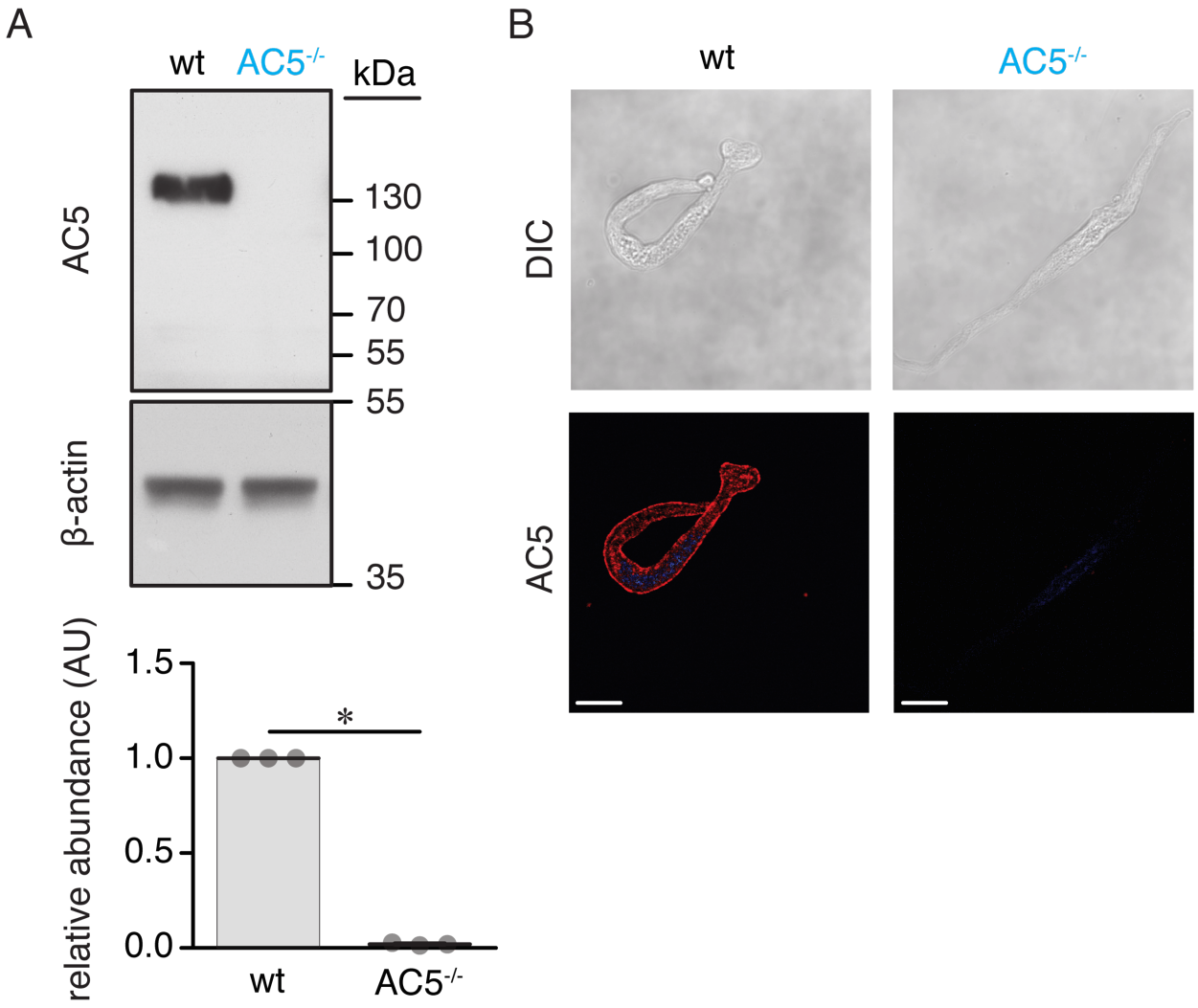

Figure S6: Expression of AC5 in brain lysates and isolated arterial myocytes. A) Representative Western blot of immunoreactive bands of expected molecular mass for AC5 (~130 kDa) and corresponding β-actin (~35-40 kDa) (*top panel*) in whole brain lysates from wild type and AC5$^{-/-}$ mice. The *lower panel* shows amalgamated densitometry data (mean ± SEM) for AC5 abundance in wild type (n = 3 lysates) and AC5$^{-/-}$ (n = 3 lysates) lysates relative to β-actin. *P < 0.05, Mann-Whitney test. **B)** Exemplary differential interference contrast (DIC) and confocal fluorescence (merged Alexa 488 and DAPI) images of AC5 in isolated wild type and AC5$^{-/-}$ arterial myocytes (scale bar = 10 µm; n = 5 cells per condition). Data are represented as mean ± SEM.

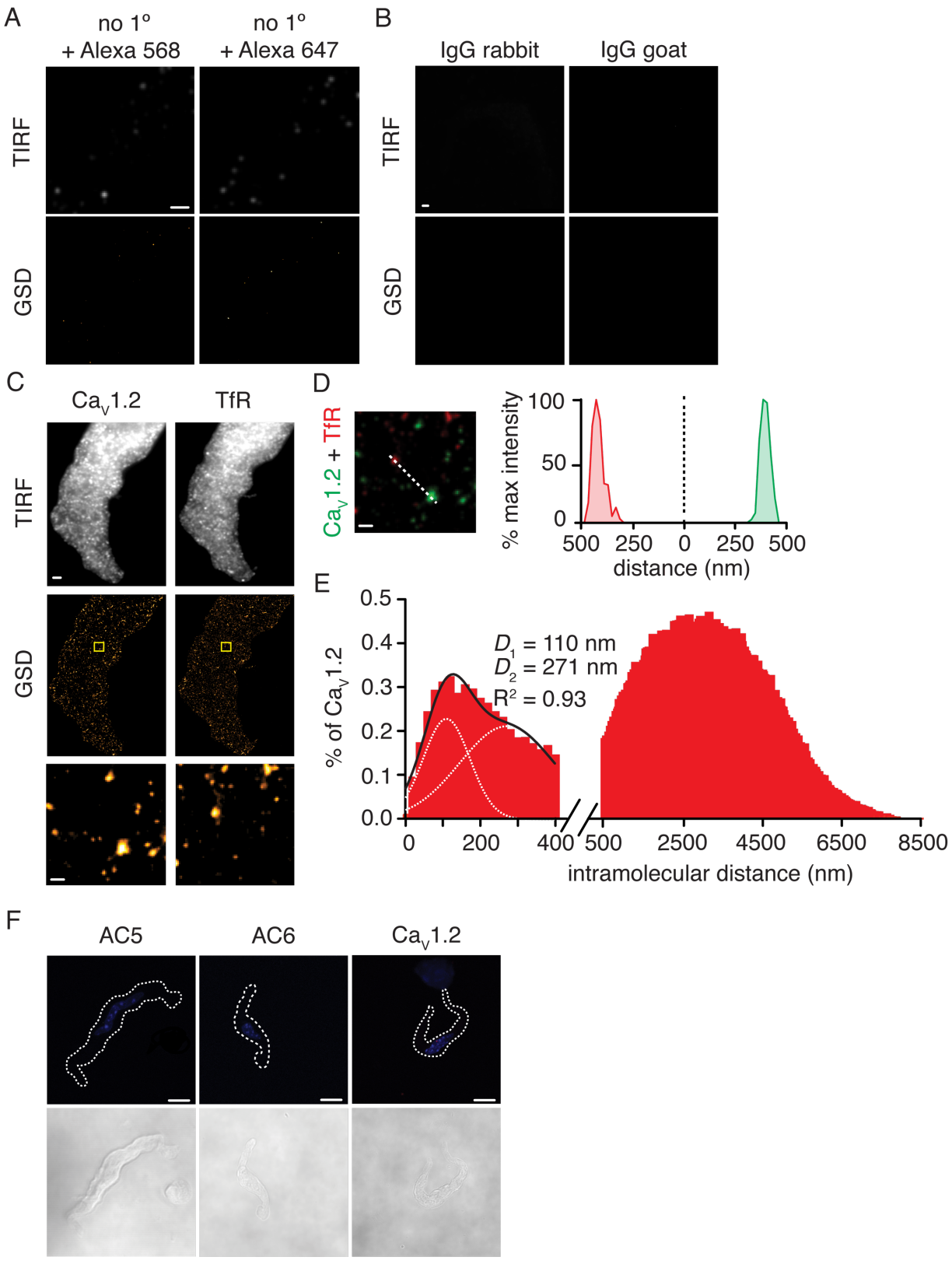
A
no 1°
+ Alexa 568
no 1°
+ Alexa 647
TIRF
GSD
B
IgG rabbit
IgG goat
TIRF
GSD
C
$Ca_V1.2$
TfR
TIRF
GSD
D
$Ca_V1.2$ + TfR
% max intensity
100
50
0
500 250 0 250 500
distance (nm)
E
% of $Ca_V1.2$
0.5
0.4
0.3
0.2
0.1
0.0
D_1 = 110 nm
D_2 = 271 nm
R^2 = 0.93
0 200 400 500 2500 4500 6500 8500
intramolecular distance (nm)
F
AC5
AC6
$Ca_V1.2$

Figure S7: Negative controls for super-resolution imaging and PLA analysis.
Representative TIRF images (*top*) and corresponding GSD reconstruction maps (*bottom*) from wild type arterial myocytes labeled with (**A**) secondary antibodies only (no 1° + Alexa 568 and no 1° + Alexa 647; scale bar = 1 µm; n = 5 cells per condition) or (**B**) corresponding primary IgG control (scale bar = 1 µm; n = 5 cells per condition). **C)** Representative TIRF images (*top*) and corresponding GSD reconstruction maps (*bottom*) from a wild type arterial myocyte labeled for $Ca_V1.2$ and transferrin receptors (TfR; n = 6 cells; scale bar = 1 µm). Higher magnification of the areas in the yellow boxes are shown in the lower panels (scale bar = 200 nm). **D)** Higher magnification of a merged image and associated *x-y* fluorescence intensity profile from the dotted line over a $Ca_V1.2$ (green) and a TfR (red) cluster (scale bar = 100 nm). **E)** Histogram of the lowest intermolecular distance to TfR centroids for $Ca_V1.2$ particles. Data were fit with a multi-Gaussian function (n = 275,157 particles from 6 cells). **F)** Exemplary confocal PLA and differential interference contrast (DIC) images of freshly dissociated arterial myocytes labeled with a primary antibody only for AC5 (*left panels*), AC6 (*middle panels*) and $Ca_V1.2$ (*right panels*) (scale bar = 10 µm; n = 18-22 cells per condition).

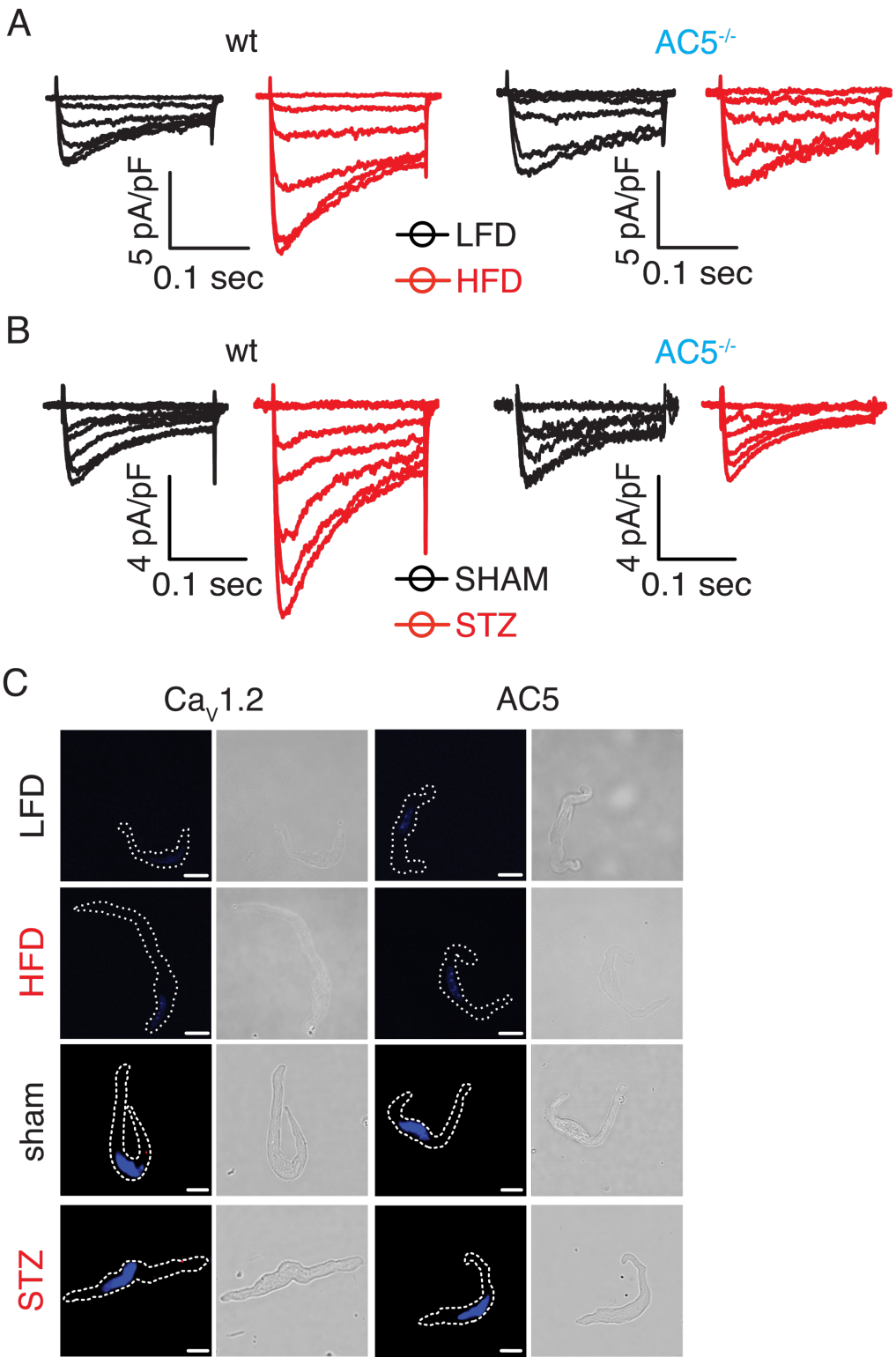

Figure S8: I_{Ba} recordings and negative controls for PLA analysis from LFD/HFD and sham/STZ wild type and AC5$^{-/-}$ arterial myocytes. Exemplary nifedipine-sensitive I_{Ba} traces evoked over a range of voltages (-40 to +50 mV) in arterial myocytes from wild type and AC5$^{-/-}$

mice in (**A**) LFD/HFD and (**B**) sham/STZ. For simplicity, only traces obtained at -60, -40, -20, +10, +30 and +50 mV are shown. **C)** Representative confocal PLA and differential interference contrast (DIC) images of wild type arterial myocytes isolated from LFD/HFD and sham/STZ mice labeled with a primary antibody only for $Ca_V1.2$ or AC5 (scale bar = 10 µm).

Table S1: Arterial diameter data for experiments in Figure 1A

treatment	**diameter (μm)**					
artery	1	2	3	4	5	6
5 mM D-glu	133	66	101	127	55	135
10 mM D-glu	134	66	100	128	54	135
15 mM D-glu	127	60	86	111	30	121
20 mM D-glu	123	52	88	109	26	111
30 mM D-glu	123	52	88	109	30	113
40 mM D-glu	122	51	88	109	30	110
passive	143	98	135	165	112	153

Table S2: Percent treatment-induced changes in arterial tone for experiments in Figure 1A

[D-glu] (mM)	Δ arterial tone (%)
5	0.0 ± 0.0
10	0.2 ± 0.2
15	10.4 ± 2.6
20	13.9 ± 2.7*
30	13.1 ± 2.2*
40	13.7 ± 2.2*

Values are mean ± SEM. *P < 0.05 with Kruskal-Wallis with Dunn's multiple comparisons.

Table S3: Arterial diameter data for experiments in Figure 2E-2G and Figure S3

treatment	diameter (µm)					
- 2,5 DDA experiments						
artery	1	2	3	4	5	6
10 mM D-glu at 20 mmHg	105	120	129	100	126	116
60 mM K^+	36	30	33	48	53	25
10 mM D-glu at 60 mmHg	109	105	140	136	115	119
20 mM D-glu at 60 mmHg	101	90	126	125	102	104
forskolin	130	110	155	158	140	140
passive	135	118	165	163	144	141
+ 2,5 DDA experiments						
10 mM D-glu at 20 mmHg	139	119	139	117	140	121
60 mM K^+	54	47	56	51	28	42
- 2,5 DDA / 10 mM D-glu at 60 mmHg	122	120	134	109	109	124
+ 2,5 DDA / 10 mM D-glu	124	127	134	119	119	119
+ 2,5 DDA / 20 mM D-glu	127	125	131	118	124	125
forskolin	179	147	165	141	147	145
passive	180	151	167	141	150	157

Table S4: Percent treatment-induced changes in diameter for experiments in Figure 2E-2G and Figure S3

	- 2,5 DDA	**+ 2,5 DDA**
peak 60 mM K^+ constriction (%)	67.3 ± 4.1	63.8 ± 3.4
arterial tone (%) in 10 mM D-glu	16.3 ± 1.5	21.2 ± 2.4
arterial tone (%) in 20 mM D-glu	25.2 ± 1.0$^{\#}$	20.4 ± 2.0
Δ arterial tone/diameter in 20 mM D-glu (%)	8.9 ± 1.0*	-0.8 ± 1.0
Δ arterial diameter in 20 mM D-glu + forskolin (%)	22.2 ± 1.5	18.4 ± 2.3

Values are mean ± SEM. *P < 0.05 with Mann-Whitney test for comparison of Δ arterial tone (%) in 20 mM D-glu between the -2,5 DDA and +2,5 DDA. $^{\#}P$ < 0.05 with Wilcoxon matched-pairs signed rank test for comparison between 10 mM D-glu vs. 20 mM D-glu for each group.

Table S5: Arterial diameter data for experiments in Figure 3E-3F and Figure S5

treatment	diameter (µm)								
wild type									
artery	1	2	3	4	5	6	7	8	9
10 mM D-glu at 20 mmHg	130	116	115	102	132	84	152	-	-
60 mM K^+	35	28	37	35	16	29	54	-	-
10 mM D-glu at 60 mmHg	122	138	110	123	130	85	157	-	-
20 mM D-glu at 60 mmHg	96	124	87	11	122	65	140	-	-
forskolin	140	131	125	150	148	105	175	-	-
passive	141	164	129	153	152	108	177	-	-
$AC5^{-/-}$									
10 mM D-glu at 20 mmHg	103	100	108	112	104	110	95	-	-
60 mM K^+	36	52	12	28	15	39	20	-	-
10 mM D-glu at 60 mmHg	86	115	115	107	103	94	105	-	-
20 mM D-glu at 60 mmHg	87	114	120	106	101	94	101	-	-
forskolin	112	137	132	142	129	130	122	-	-
passive	126	147	136	142	129	137	122	-	-
$AC5^{-/+}$									
10 mM D-glu at 20 mmHg	111	100	140	130	94	70	120	112	134
60 mM K^+	49	45	69	50	49	29	50	54	45
10 mM D-glu at 60 mmHg	125	120	146	142	97	108	114	116	96
20 mM D-glu at 60 mmHg	99	110	113	119	82	97	99	107	85
forskolin	146	133	163	159	109	126	152	137	121

passive	152	133	164	163	109	126	153	138	121
AC6$^{-/-}$									
10 mM D-glu at 20 mmHg	160	136	102	115	110	-	-	-	-
60 mM K^+	28	71	23	50	62	-	-	-	-
10 mM D-glu at 60 mmHg	151	156	86	113	120	-	-	-	-
20 mM D-glu at 60 mmHg	127	150	73	104	107	-	-	-	-
passive	179	170	114	129	133	-	-	-	-

Table S6: Percent treatment-induced changes in diameter for experiments in Figure 3E-3F and Figure S5

	wild type	AC5$^{-/-}$	AC5$^{-/+}$	AC6$^{-/-}$
peak 60 mM K^+ constriction (%)	71.5 ± 3.2	72.3 ± 5.4	56.2 ± 1.7	61.6 ± 7.8
arterial tone in 10 mM D-glu (%)	15.8 ± 1.3	22.9 ± 2.7	15.5 ± 1.7	14.1 ± 2.9
arterial tone in 20 mM D-glu (%)	28.1 ± 2.7$^{\#}$	23.0 ± 2.7	27.3 ± 1.7$^{\#}$	23.1 ± 4.2$^{\#}$
Δ arterial tone/diameter in 20 mM D-glu (%)	12.3 ± 2.2*	0.2 ± 0.8	11.9 ± 1.6*	-
Δ arterial diameter in 20 mM D-glu + forskolin (%)	24.1 ± 4.1	20.0 ± 2.4	26.6 ± 1.9	-

Values are mean ± SEM. *P < 0.05 with Kruskal-Wallis with Dunn's multiple comparison test for Δ arterial tone (%) between the wild type, AC5$^{-/-}$, AC5$^{-/+}$ and AC6$^{-/-}$. $^{\#}P$ < 0.05 with Wilcoxon matched-pairs signed rank test or Paired t-test for comparison between 10 mM D-glu vs. 20 mM D-glu for each group.

Table S7: Arterial diameter data for experiments in Figure 4

treatment	diameter (pixels)							
wild type								
artery	1	2	3	4	5	6	7	8
10 mM D-glu	7.3	7.6	7.7	6.8	9.0	8.1	8.6	17.0
20 mM D-glu	4.6	4.1	3.7	5.5	10.1	6.7	6.0	13.0
10 mM D-glu + 10 mM mannitol	7.3	7.2	7.0	6.7	10.0	8.1	8.6	16.4
passive	10.5	9.7	7.9	10.1	16.0	13.6	11.7	19.1
AC5$^{-/-}$								
10 mM D-glu	11.4	5.6	3.7	7.3	10.8	8.7	9.3	8.9
20 mM D-glu	11.9	6.7	4.2	7.5	11.9	8.1	9.4	8.3
10 mM D-glu + 10 mM mannitol	12.3	5.7	4.5	7.3	12.3	9.4	8.3	10.1
passive	14.6	7.2	6.7	9.0	14.6	11.5	11.8	14.1

Table S8: Percent treatment-induced changes in diameter for experiments in Figure 4

	wild type	AC5$^{-/-}$
arterial tone in 10 mM D-glu (%)	26.0 ± 5.0	27.1 ± 3.2
arterial tone in 20 mM D-glu (%)	47.4 ± 3.2*	23.6 ± 4.1
arterial tone in 10 mM D-glu +10 mM mannitol (%)	27.3 ± 3.8	22.4 ± 2.3

Values are mean ± SEM. *P < 0.05 with ANOVA with Tukey's multiple comparisons test within each group.

Table S9: Metabolic characterization of LFD and HFD mice

parameters measured	wt LFD	wt HFD	AC5$^{-/-}$ LFD	AC5$^{-/-}$ HFD
body weight (g)	30.1 ± 1.7	44.5 ± 2.3*	25.1 ± 2.2	39.1 ± 2.3*
non-fasting glucose (mg/dL)	140.8 ± 11.7	245.0 ± 10.2*	144.9 ± 12.7	256.4± 17.9*
insulin (pg/ml)	853 ± 35	4341 ± 2245 (*P* = 0.0635)	1231 ± 325	3420 ± 1235*
cholesterol (mg/dL)	121.6 ± 28.7	227.0 ± 15.4*	118.3 ± 5.7	191.5 ± 20.2*

Values are mean ± SEM. *$P < 0.05$ with Mann-Whitney test between LFD and HFD for all groups.

Table S10: Metabolic characterization of sham and STZ mice

parameters measured	wt sham	wt STZ	AC5$^{-/-}$ sham	AC5$^{-/-}$ STZ
body weight (g)	28.0 ± 1.2	25.0 ± 2.1	27.0 ± 1.2	22.0 ± 1.1*
non-fasting glucose (mg/dL)	159.2 ± 10.1	445.8 ± 40.2*	133.8 ± 4.4	533.1 ± 38.2*
insulin (pg/ml)	851.5 ± 157.5	554.8 ± 136.4 (P = 0.1320)	971.8 ± 273.8	272.0 ± 64.4*
cholesterol (mg/dL)	112.4 ± 11.7	118.4 ± 3.8	79.4 ± 12.2	93.3 ± 13.5

Values are mean ± SEM. *P < 0.05 with Mann-Whitney test between sham and STZ for all groups.

Table S11: Arterial diameter data for experiments in Figure 7A-7B

treatment	diameter (μm)					
wild type LFD						
	artery 1	artery 2	artery 3	artery 4	artery 5	artery 6
60 mM K^+	49	37	40	25	54	55
10 mmHg	121	131	115	98	119	122
20 mmHg	128	141	115	104	125	122
40 mmHg	124	145	124	118	141	135
60 mmHg	128	143	130	110	129	134
80 mmHg	137	153	137	117	141	148
100 mmHg	141	158	142	118	143	150
passive diameter						
10 mmHg	121	135	115	99	120	127
20 mmHg	124	145	126	116	137	137
40 mmHg	136	167	140	131	142	151
60 mmHg	156	172	144	136	150	160
80 mmHg	166	175	147	138	161	170
100 mmHg	169	176	149	138	166	173
wild type HFD						
	artery 1	artery 2	artery 3	artery 4	artery 5	artery 6
60 mM K^+	24	28	16	28	35	37
10 mmHg	103	78	131	78	109	98
20 mmHg	105	81	137	81	116	105

40 mmHg	114	84	132	84	113	99
60 mmHg	121	91	133	91	112	96
80 mmHg	119	84	155	84	115	106
100 mmHg	112	94	160	88	112	99
passive diameter						
10 mmHg	113	98	146	98	119	99
20 mmHg	126	102	160	102	135	110
40 mmHg	147	108	178	108	150	117
60 mmHg	155	110	188	110	155	119
80 mmHg	160	110	189	110	156	119
100 mmHg	160	110	191	110	158	120
$AC5^{-/-}$ LFD						
	artery 1	artery 2	artery 3	artery 4	artery 5	artery 6
60 mM K^+	30	35	28	13	28	13
10 mmHg	91	112	100	55	115	63
20 mmHg	99	113	109	56	123	61
40 mmHg	115	112	110	66	136	71
60 mmHg	107	119	130	60	141	73
80 mmHg	110	121	134	64	145	80
100 mmHg	114	127	135	65	149	80
passive diameter						
10 mmHg	98	119	114	55	123	63
20 mmHg	120	134	125	62	134	63

40 mmHg	138	148	147	76	149	74
60 mmHg	139	154	154	83	159	81
80 mmHg	140	155	155	83	159	84
100 mmHg	143	156	157	85	161	84
$AC5^{-/-}$ HFD						
	artery 1	artery 2	artery 3	artery 4	artery 5	artery 6
60 mM K^+	16	62	57	46	34	40
10 mmHg	101	109	100	113	99	95
20 mmHg	96	120	118	119	112	100
40 mmHg	97	126	124	130	119	106
60 mmHg	93	132	132	138	123	112
80 mmHg	109	135	136	144	111	123
100 mmHg	119	138	141	145	131	123
passive diameter						
10 mmHg	106	120	130	114	125	107
20 mmHg	118	120	142	137	133	124
40 mmHg	129	134	155	151	141	143
60 mmHg	134	152	155	154	146	156
80 mmHg	136	154	160	155	148	161
100 mmHg	140	158	162	156	150	165

Table S12: Percent treatment-induced changes in diameter for experiments in Figure 7A-7B

	wild type		**AC5$^{-/-}$**	
	LFD	HFD	LFD	HFD
peak 60 mM K^+ constriction (%)	61 ± 4	75 ± 4*	74 ± 2	61 ± 7
% arterial tone at given intravascular pressure				
10 mmHg	1.3 ± 0.7	11.6 ± 3.1	5.3 ± 1.9	11.6 ± 3.6
20 mmHg	6.4 ± 2.3	15.1 ± 2.4*	11.2 ± 2.1	14.0 ± 2.9
40 mmHg	9.1 ± 1.8	22.1 ± 1.5*	15.4 ± 3.4	17.7 ± 3.0
60 mmHg	15.7 ± 1.4	22.1 ± 2.1*	18.4 ± 2.9	18.8 ± 3.4
80 mmHg	12.9 ± 1.5	21.4 ± 2.4*	15.6 ± 3.1	17.2 ± 2.8
100 mmHg	12.2 ± 1.7	21.2 ± 2.7*	14.8 ± 3.0	14.3 ± 2.5

Values are mean ± SEM. *$P < 0.05$ with Mann-Whitney test for each group.

Table S13: Arterial diameter data for experiments in Figure 7C

wild type sham			
mouse ID: 429	**diameter (pixels)**		
artery #	**baseline**	**passive**	**% tone**
1	5.1	5.7	10.5
2	6.5	7.8	16.7
3	4.8	6.3	23.8
4	6.2	7.4	16.2
5	6.3	7.3	13.7
6	3.7	4.6	19.6
7	6.1	6.6	7.6
mouse ID: 431			
1	12.2	14.6	16.4
2	10.2	12.5	18.4
3	5.2	6.7	22.4
4	5.0	7.2	30.6
5	6.1	8.2	25.6
6	4.6	7.0	34.3
mouse ID: 432			
1	11	13.5	18.5
2	7.6	9.3	18.3
3	7.2	8.5	15.3
4	3.5	5.6	37.5
5	6.5	8.0	18.8
6	6.8	9.4	27.7

mouse ID: 439			
1	13.2	14.9	11.4
2	8.0	10.1	20.8
3	5.2	6.3	17.5
4	4.1	5.0	18.0
5	5.5	8.0	31.3
6	8.9	10.0	11.0
mouse ID: 441			
1	10.6	11.6	8.7
2	5.4	7.0	22.3
3	6.1	7.8	22.2
4	7.0	11.0	36.8
5	5.0	8.0	37.5
6	7.0	8.2	14.8
7	4.3	5.9	27.4
8	6.6	7.1	7.8
9	9.2	10.4	11.8
10	5.8	6.9	15.4
11	6.7	9.3	28.0
wild type STZ			
mouse ID: 436			
1	10.0	13.3	24.8
2	6.7	11.9	43.7
3	3.8	8.2	53.7
4	4.0	9.4	57.4

5	5.1	7.0	27.1
6	6.0	10.0	40.0
7	4.3	8.7	50.6
8	6.2	8.5	27.1
9	6.8	11.0	38.2
10	5.5	7.7	28.6
11	4.2	5.2	19.2
12	4.0	7.8	48.7
13	6.1	8.5	28.2
14	4.9	11.1	55.9
15	2.7	4.5	40.0
mouse ID: 437			
1	14.6	16.7	12.6
2	13.5	17.9	24.6
3	11.3	16.0	29.4
4	10.9	13.1	16.8
5	8.3	12.3	32.5
6	1.9	5.7	66.7
7	6.9	8.5	18.8
8	9.2	12.5	26.4
9	2.5	5.5	54.5
10	2.5	6.2	59.7
11	1.8	5.1	64.7
12	1.5	6.4	76.6
mouse ID: 438			

1	7.8	10.7	27.10280374
mouse ID: 446			
1	14.0	19.5	28.2
2	9.0	13.0	30.8
3	8.5	15.1	43.7
4	6.0	10.3	41.7
5	6.5	10.8	39.8
6	7.5	10.1	25.7
7	2.8	7.1	60.6
8	2.3	6.9	66.7
9	5.0	8.5	41.2
10	6.1	9.2	33.7
11	3.2	6.0	46.7
12	3.7	6.7	44.8
13	4.4	7.4	40.5
14	1.0	6.1	83.6
15	2.5	5.2	51.9
16	4.8	7.0	31.4
17	2.9	5.7	49.1
mouse ID: 448			
1	10.8	15.9	32.1
2	6.4	8.9	28.1
3	9.7	12.8	24.2
4	4.8	8.2	41.5
5	4.5	7.4	39.2

6	4.8	9.9	51.5
7	5.7	11.8	51.7
8	2.4	4.8	50.0
9	6.5	8.6	24.4
10	6.0	11.3	46.9
11	7.6	9.1	16.5
12	7.9	13.0	39.2
13	4.9	9.1	46.2
14	4.5	8.1	44.4
15	2.2	5.5	60.0
16	7.3	11.7	37.6
17	9.4	16.0	41.3
18	7.2	13.5	46.7
19	2.8	4.4	36.4
20	6.7	9.1	26.4
21	2.8	5.3	47.2
22	4.6	9.1	49.5
mouse ID: 445			
1	12.2	13.9	11.7
2	7.9	11.5	31.0
3	8.6	12.9	33.5
4	5.8	6.9	17.0
5	8.2	11.0	25.8
6	4.7	8.1	42.6
7	9.3	13.0	28.3

8	6.7	12.4	46.4
9	4.5	9.3	51.0
10	6.0	9.0	33.3
$AC5^{-/-}$ sham			
mouse ID: 415	**diameter (pixels)**		
1	12	14.5	17.2
2	7.1	9.8	27.6
3	5.7	8	28.8
4	6.1	8.1	24.7
5	6	7.9	24.1
6	7.3	8.7	16.1
7	6.8	8.9	23.6
8	3	5.8	48.3
9	6	7.8	23.1
10	8	9.4	14.9
11	8.9	10.1	11.9
mouse ID: 815			
1	10.1	11.1	9.0
2	10.9	12.5	12.8
3	5.4	8.3	34.9
4	4.4	5.6	21.4
5	6.0	6.7	10.4

mouse ID: 1661			
1	11.0	14.2	22.8
2	10.6	12.7	16.3
3	7.6	10.2	24.8
4	6.7	8.9	25.0
5	5.1	5.5	7.7
6	8.1	8.5	5.3
7	9.1	10.6	14.2
8	5.0	9.2	46.1
9	7.6	10.3	26.5
10	7.4	8.6	14.5
11	4.5	9.1	50.3
12	2.7	4.6	39.6
mouse ID: 1662			
1	6.0	8.1	26.2
2	4.9	7.8	37.6
3	5.4	8.4	36.2
4	13.1	17.3	24.2
5	7.3	11.1	33.7
6	7.9	12.1	35.2
7	7.6	11.4	33.6
8	8.9	11.8	24.1
9	5.1	6.4	20.5
10	7.1	8.7	17.9
$AC5^{-/-}$ STZ			

mouse ID: 1519			
1	10.8	12.2	11.5
2	4.3	5.7	24.6
3	5.0	5.9	15.3
4	9.2	10.6	13.2
5	7.5	9.0	16.7
6	5.9	7.3	19.2
7	4.8	7.5	36.0
8	5.6	6.9	18.8
9	3.5	5.0	30.0
10	4.8	6.7	28.4
11	2.6	3.7	29.7
12	12.0	13.0	7.7
13	8.0	8.5	5.9
14	7.6	7.8	2.6
mouse ID: 1663			
1	3.5	4.6	23.9
2	4.8	4.9	2.0
3	4.7	5.1	7.8
4	6.3	8.9	29.2
5	3.5	6.4	45.3
6	6.7	8.2	18.3
7	5.0	6.1	18.0
8	3.8	6.2	38.7
mouse ID: 1666			

1	8.0	10.4	23.1
2	6.0	7.2	16.7
3	5.8	7.0	17.1
4	7.6	11.2	32.1
5	5.5	6.4	14.1
6	3.6	5.7	36.8
7	5.5	7.5	26.7

mouse ID: 1664			
1	5.4	8.8	38.7
2	6.3	10.0	36.7
3	4.5	7.4	40.1
4	3.1	8.8	64.5
5	6.2	8.9	30.3
6	4.0	7.6	47.2
7	6.7	9.0	25.9
8	5.5	7.9	30.2
9	5.0	7.7	34.5
10	7.7	10.3	25.8
mouse ID: 1665			
1	13.5	14.2	4.6
2	9.5	11.9	19.6
3	9.9	11.6	14.9
4	4.9	6.3	22.9
5	9.3	11.1	16.7

6	6.2	9.0	31.2
7	6.2	8.1	23.2
8	7.8	10.1	23.3
9	11.1	11.7	5.1
10	5.3	6.9	23.5
11	6.5	8.8	25.6
12	6.2	6.5	4.8
mouse ID: 838			
1	7.6	8.8	13.6
2	9.0	9.1	1.1
3	8.1	8.2	1.2
4	6.0	6.3	4.8
5	6.5	7.1	8.5
6	7.3	7.5	2.7
7	3.7	5.3	30.2
8	5.4	7.0	22.9
9	4.0	5.5	27.3
10	5.5	6.3	12.7
11	6.4	7.3	12.3
12	4.3	6.7	35.8
mouse ID: 839			
1	12.5	14.4	13.4
2	8.2	10.1	19.2
3	9.3	11.0	14.8
4	6.5	8.5	23.6

5	9.4	10.7	12.0
6	7.3	8.8	17.7
7	4.6	6.6	30.2
8	5.8	9.1	36.0
9	5.2	7.9	33.6
10	4.7	6.3	24.5

Table S14: Percent treatment-induced changes in myogenic tone for experiments in Figure 7C

treatment	wild type	AC5$^{-/-}$
sham	20.4 ± 1.4	24.5 ± 1.8
STZ	39.7 ± 1.7*	21.9 ± 1.5

Values are mean ± SEM. *P < 0.05 with Mann-Whitney test for each group.

Table S15: Key reagents/resources used in the study

Reagent type (species) or resource	Designation	Source or reference	Identifiers	Additional Information
strain (*Mus musculus*), C57BL/6J	wild-type	Jackson Laboratories	stock # 000664	
strain (*Mus musculus*)	$AC5^{-/-}$	(1)		Backcrossed for 10 generations into the C57BL/6J background
strain (*Mus musculus*)	$AC6^{-/-}$	(1)		Backcrossed for 10 generations into the C57BL/6J background
strain (*Mus musculus*)	$AC5^{-/+}$			Generated for this study by crossing C57BL/6J with $AC5^{-/-}$ mice
antibody	anti-FP1 ($Ca_V1.2$; custom rabbit)	(17)		dilutions: 1:100 for immunoblot and PLA; 10 µg/mL for GSD
antibody	anti-AC5 (goat polyclonal)	Santa Cruz Biotechnology	sc74301 RRID: AB_2289217	1:50-1:1000 dilutions
antibody	anti-β-actin (mouse monoclonal)	Abcam	ab8226 RRID: AB_30637	1:1000 dilution
antibody	anti-TfR (mouse monoclonal)	ThermoFisher Scientific	13-6800 RRID: AB_2533029	1:1000 dilutions
antibody	Alexa Fluor 488-conjugated donkey anti-goat	Molecular Probes	A11055 RRID: AB_142672	5 mg/mL dilution
antibody	Alexa Fluor 568-conjugated donkey anti-rabbit	Molecular Probes	A11011 RRID: AB_143157	2 µg/mL dilution

antibody	Alexa Fluor 647-conjugated donkey anti-goat	Molecular Probes	A21447 RRID: 141844	2 µg/mL dilution
antibody	goat anti-mouse IgG (H+L)-horseradish peroxidase conjugate	Bio-Rad	STAR132P RRID: AB_2124272	1:10000 dilution
antibody	donkey anti-goat IgG (H+L)-horseradish peroxidase conjugate	Bio-Rad	642004 RRID: AB_609688	1:10000 dilution
antibody	alpha-smooth muscle actin - Alexa Fluor 488	Abcam	ab197240 clone # E184	
antibody	CD90.2 (Thy1.2)-phytoerythrin	BD Bioscience	553005 RRID: AB_394544	
antibody	CD31 - biotin	BD Bioscience	558737 RRID: AB_397096	
antibody	CD45 - biotin	BD Bioscience	553077 RRID: AB_394607	
antibody	lineage antibody cocktail	BD Bioscience	559971 RRID: AB_10053179	
antibody	streptavidin - AlexaFluor 750 allophycocyanin conjugate secondary antibody	ThermoFisher Scientific	S21008	
antibody	rabbit IgG	Jackson ImmunoResearch	011-000-003 RRID: AB_2337118	10 µg/mL dilution
antibody	goat IgG	Jackson ImmunoResearch	005-000-003 RRID: AB_2336985	10 µg/mL dilution

chemical compound, drug	sodium pentobarbital (Fatal-Plus)	Vortech Pharma-ceuticals	NDC 0298-9373-68	
chemical compound, drug	mannitol	Fisher Scientific	BP686	
chemical compound, drug	nifedipine	Sigma-Aldrich	N7634	
chemical compound, drug	forskolin	Sigma-Aldrich	F6886	
chemical compound, drug	amphotericin B	Sigma-Aldrich	A4888	
chemical compound, drug	2,5 DDA	Sigma-Aldrich	D7408	
chemical compound, drug	streptozocin	Sigma-Aldrich	S0130	
calcium indicator	Fluo-4 AM	ThermoFisher Scientific	F14201	cell permeant
calcium indicator	Cal-520 AM	AAT Bioquest	21130	cell permeant
FRET biosensor	ICUE3-PM/ ICUE3-NLS	(12, 13)		viruses/DNA constructs
transfection reagent	TransferX	ATCC	ACS-4005	
diet	10% kcal fat	Research Diets	D12450J	
diet	60% kcal fat	Research Diets	D12492	
software, algorithm	GraphPad Prism		GraphPad Prism, RRID: SCR_002798	
software, algorithm	ImageJ		Fiji, RRID: SCR_002285	
software, algorithm	pCLAMP10	Molecular Devices		electrophysiology
software, algorithm	LASAF	Leica		GSD
software, algorithm	IonOptix	IonOptix		arterial diameter recordings

software, algorithm	Metaflor	Molecular Devices		FRET
software, algorithm	custom software		somapp.ucdmc.ucdavis.edu/Pharmacology/bers	*in silico* data
software, algorithm	custom software		elegrandi.wixsite.com/grandilab/downloads	*in silico* data